Future risk of decadal megadrought events over eastern China based on IPO-constrained precipitation

Liang Ning (✉ ningliangnnu@njnu.edu.cn)

Nanjing Normal University

Yanmin Qin

Nanjing Normal University

Longhui Li

Nanjing Normal University

Jian Liu

Nanjing Normal University

Mi Yan

Nanjing Normal University

zhengyu Liu

the Ohio State University

Guonian Lv

Nanjing Normal University

Linwang Yuan

Nanjing Normal University

Kefan Chen

Nanjing Normal University

Weiyi Sun

Nanjing Normal University

Qin Wen

Nanjing Normal University

Jiao Xue

Nanjing Normal University

Liulin Wang

Nanjing Normal University

Chuxin Li

Nanjing Normal University

Article

Keywords:

Abstract

A reliable projection of future risk of decadal megadrought event is crucial for adaption and mitigation over eastern China to future climate changes. However, large uncertainties are induced by emission scenarios, model structures, and internal variability in current model simulation. Using a 50-member ensemble of simulations from the Community Earth System Model Version 2 Large Ensemble (CESM2-LE), it is found that, under the same emission scenario, internal variability contributes a large part to the total uncertainties of decadal precipitation variability over eastern China, and the interdecadal Pacific oscillation (IPO), could contribute about 30% to internal uncertainty during future period (2021–2080). Then, an emergent constraint based on IPO is applied to the model simulated precipitation. Finally, constrained precipitation changes show that northern China will have a high megadrought risk in the 2050s to 2060s, and Yangtze River Valley will have a high megadrought risk in the 2030s to 2040s. These will have great benefit to specific strategies of social infrastructure in the future.

Introduction

With a large population and rapid developments, eastern China is vulnerable to extreme drought events, which raise severe impacts on agriculture, natural environment, and human society[1,2]. As the Sixth Assessment Report of the Intergovernmental Panel on Climate Change (IPCC AR6) concluded, anthropogenic influence induces global climate change since pre-industrial period unequivocally[3]. Model simulation suggest an increased risk of megadrought around the world under global warming in this century[4–7], highlighting the importance of mitigation of future warming[4,8,9]. Especially, eastern China will be confronted with the same increasing megadrought condition under a projected high emission scenario[10–12]. Thus, a reliable projection and early warning of decadal megadrought events are crucial for eastern China[13,14].

Coupled Model Intercomparison Project Phase 6 (CMIP6) model simulations project precipitation increase over East Asian summer monsoon (EASM) region due to the greenhouse gases (GHGs)-induced "the Northern Hemisphere warmer than the Southern Hemisphere" and "land warmer than ocean" patterns[15]. However, there remains large uncertainties in future precipitation projection[16], which impend accurate estimation of future megadrought in decadal time scale[17,18]. Previous studies show that internal variability of the climate system, model structure difference, and future scenarios of GHGs emissions are the three main sources of uncertainty in model projection[19,20]. Superimposed by complex interactions between sea surface temperature (SST) and atmospheric circulation, these sources cause a large uncertainty on projected megadrought over eastern China[21–23].Moreover, regional megadrought is strongly affected by both internal variability and external forcing, through inducing local circulation changes[24–27]. Based on proxy reconstructions and model simulations during last millennium, historical megadroughts over eastern China are mainly trigged by internal variability and modulated by natural and anthropogenic forcings, e.g., volcanic eruption, solar radiation, anthropogenic aerosol and GHGs

emissions[28–31]. Thus, reducing the uncertainty due to internal variability will largely improve megadrought projection over eastern China.

Among the internal variability of the climate system, the Interdecadal Pacific Oscillation (IPO; ref. [32]) and Pacific Decadal Oscillation (PDO; ref. [33]), are the leading modes on decadal scale. They are found to contribute largely to regional decadal precipitation variability[34–37], especially to eastern China[38–41]. In recent decades, PDO/IPO phase shifted from positive to negative, and caused EASM weakening and the less precipitation over northern part of eastern China since the late 1970s[26,42,43]. Mechanisms analyses show that, there are negative sea level pressure (SLP) anomalies over the northwest Pacific but positive SLP anomalies over northern China during the positive PDO/IPO phase, which generates northwesterly wind anomalies over northern China and corresponding weaker EASM[25,43]. Therefore, this relationship between PDO/IPO and decadal precipitation change was also applied to the study of future regional precipitation changes over eastern China. For example, based on projected PDO/IPO trend, previous studies constrained future regional precipitation trend over the south Asia and California, Unite States effectively[44,45]. In addition, the trends of historical temperature and interhemispheric thermal contrast (ITC) were respectively used to constrain the increasing trend of future Asian precipitation[21,22]. Although plenty of constraining methods were successfully developed and applied to regional climate projections, the projections of regional megadrought risks associated with decadal precipitation variability over eastern China based on constraining methods has received little attention.

In this study, an IPO-based constraining method is applied to Community Earth System Model Version 2 Large Ensemble (CESM2-LE; ref. [46]) to project decadal precipitation variability over eastern China, and the corresponding future risk of decadal megadrought was then quantitatively estimated during the period 2021–2080. First, the uncertainty sources of simulated decadal precipitation over eastern China were recognized by ensembles from CMIP6 and CESM2-LE. Then, IPO-based-constraining precipitation was set up to project the future megadrought over eastern China. Hence, more accurate megadrought risks in northern China (NC) and Yangtze River Valley (YRV) are estimated. These results will provide scientific support related adaptation and mitigation strategies of the future climate changes.

Results

Uncertainty due to internal variability. The contributions of uncertainty due to internal variability in simulated decadal precipitation over eastern China under the same scenario are first investigated. Because the observed precipitation distribution in eastern China is the typical "flood in the south and drought in the north" (SF/ND) pattern since the late 1970s, two sub-regions, i.e., northern China (NC; $37°$-$42°$N; $112°$-$121°$E) and the Yangtze River Valley (YRV; $28°$-$32°$N;$115°$-$121°$E) were identified as two representative regions in this study.

The total uncertainties and uncertainty due to internal variability in precipitation variability based on multi-model ensemble from CMIP6 and multi-member ensemble from the CESM2-LE are shown in Fig. 1a-

c. The uncertainty due to internal variability is comparable to the total uncertainty in both NC and YRV. In particular, the internal uncertainty is slightly larger than the total uncertainty in NC, which is related to the sample size of the model and members used in this study. It's indicated that internal variability is the one major factor contributing to the uncertainty of simulated precipitation variability over eastern China. Projected precipitation variability during future period (2021–2080) also shows similar characteristics (Supplementary Fig. 1).

Ensemble mean precipitation changes from CESM2-LE simulate the increasing trends over NC and YRV under the SSP3-7.0 scenario (Fig. 1d&e). However, the decadal scale variability in different members are quite different due to random initial conditions (Fig. 1d&e). Projection of the decadal megadrought risks over eastern China seems to be challenging. Therefore, it is necessary to quantify the uncertainty contribution from internal variability, and reduce this part of uncertainty through the emergent constraint.

To quantitatively distinguish the contribution from the internal uncertainty, the simulations from CESM2-LE are only included in the following analyses. We first regress the 50 members' SST onto NC and YRV precipitation, respectively. As shown in Fig. 2a-b, significant IPO pattern could be identified, especially on the three sub-basins used for IPO definition.

To approve the relationship between IPO and decadal precipitation variability over eastern China in CESM2-LE simulation, corresponding observed precipitation anomalies over eastern China are composited according to different historical IPO phases (Supplementary Fig. 2a-c). It's shown that positive (negative) IPO phase induces "SF/ND" ("SD/NF") precipitation pattern over eastern China. This is consistent with previous studies that the positive IPO phase potentially causes "SF/ND" precipitation pattern over eastern China during recent decades[47,48]. Therefore, it is reasonable to hypothesize that, if the uncertainty due to IPO in the model simulations is removed, the decadal precipitation variability over eastern China will have a well-constrained effect.

Constraining the decadal precipitation by the IPO. In this section, the IPO is used to constrain the simulated NC and YRV decadal precipitation variability. First, the 50-member's standardized precipitation are regressed onto their IPO indices respectively (Supplementary Fig. 3). The simulated spatial patterns of regressions quite resemble to observation showing the opposite effect of IPO on NC and YRV precipitation. In historical period, compared with the observation (Supplementary Fig. 2), the significant simulated regressions on YRV have wider coverage associated with IPO with south to 28°N. However, the significant negative regressions with IPO move to the north to 35°N (Supplementary Fig. 3a). The region with largest regression coefficients is located between 40 to 45 °N over northeast China. In future period (2021–2080), the relationship between the IPO and NC precipitation is weaker, while the YRV is enhanced.

The averaged coefficient of determinations R^2 of 50-member ensemble are 0.156 and 0.116 for NC during historical and future periods respectively, and 0.082 and 0.085 for YRV during historical and future periods respectively (Supplementary Table 2). The smaller R^2 over YRV is smaller than that over NC in

both historical and future periods, which may be associated with the fact that the precipitation variability of YRV is larger than that of NC.

Using the constraining method, the precipitation is decomposed into IPO-related component and residual, and the contributions of IPO to NC and YRV precipitation variability are evaluated (Figs. 3a-b). In NC, both internal and IPO-related uncertainties are stable through historical period (1951–2010) without obvious trend (Fig. 3a). The mean values of internal and IPO-related uncertainties are 0.745 and 0.288, respectively. The IPO-related uncertainty accounted for about 38.7% of the internal uncertainty. In the future, with the increase of precipitation variability, the internal uncertainty increases with an average of 0.857. However, the IPO-related uncertainty decreases compared with the historical period, with an average of 0.267, contributing about 31.1% of internal uncertainty. In YRV, the trends of internal and IPO-related uncertainties are stable for both historical and future periods (Fig. 3b). the mean values of internal and IPO-related uncertainties are 0.804 and 0.287 in historical period, respectively. The IPO-related uncertainty accounted for about 35.7% of the internal uncertainty. In the future, the internal uncertainty increases to 0.931. However, the IPO-related uncertainty decreases slightly to 0.271, contributing about 29.1% of internal uncertainty.

In addition, the changes in internal uncertainties before and after the constraint are assessed (Figs. 3c-f). After removing the IPO-related uncertainty, the uncertainties decrease in both NC and YRV. In historical periods, the averaged uncertainties of NC and YRV decrease from 0.745 to 0.680, and 0.804 to 0.745, respectively. In the future, precipitation variability increases in both regions, and the averaged uncertainties of NC and YRV decrease from 0.857 to 0.822, and 0.931 to 0.893, respectively. These results are consistent with above analyses (Supplementary Fig. 3) and confirmed the regressed relationship and IPO-related uncertainty in model projection.

At the same time, it is also found that the precipitation of different members has different performances in reproducing the relationship between precipitation and IPO, with regression coefficients ranging from −0.852 to 0.337, with an average of -0.153 in NC and −0.413 to 0.719, with an average of 0.237 in YRV. Thus, it is necessary to filter out several members with satisfying performance in reproducing the relationship between simulated precipitation and IPO, to better project decadal scale precipitation evolution based on IPO variability.

Future risk of megadrought events. A reliable projected IPO index should be first constructed to constrain the future precipitation changes of 50-member. The observed IPO index is applied when constraining historical precipitation, which is closer to observation than the raw simulated precipitation (Supplementary Fig. 4). Moreover, in the future period, the simulated IPO index with a high correlation to the observed IPO index in the historical period (1951–2010) from the 50-member is selected as the most reliable projected IPO index for future precipitation constraints (Supplementary Fig. 5). The IPO index (member 41) with the highest correlation with the observed IPO index from 50-member with 0.849 ($p <$ 0.01) is first identified as the best member's IPO (BM-IPO; red line in Supplementary Fig. 5). To reduce the potential biases from single simulation, other four IPO indexes with the highest correlations with the

observed IPO index (member 18, 46, 48 and 14) are selected (gray thin lines in the Supplementary Fig. 5). Then, a weighted average of these five simulated IPO indices (the weighted averaged IPO, WA-IPO), with the weights assigned according to their respective correlation coefficients, is constructed to obtain the fitting IPO index (blue line in Supplementary Fig. 5). The correlation coefficient between WA-IPO and observed IPO during the historical period 1951–2014 reached 0.852 ($p < 0.01$), slightly higher than BM-IPO. The correlation coefficient of BM-IPO and WA-IPO is 0.841 ($p < 0.05$), indicating that they have relatively consistent changes in the future period.

Therefore, the BM-IPO and WA-IPO are then used to constrain the future decadal precipitation changes over NC and YRV from 2021–2080. As shown in Supplementary Fig. 6, before the constraint, the ensemble mean of 50-member (black lines) shows a monotonous linear increasing trend without obvious decadal variability. After the constraint, the ensemble mean of 50-member shows a slightly improved decadal variability in response to IPO phase change in each member. Moreover, 10 members with the highest regression coefficient of precipitation to BM-IPO and WA-IPO are selected (as shown in the gray thin line in Supplementary Fig. 7), which have the significant responses to future IPO changes. The constrained effect is obvious in the ensemble mean precipitation of these best 10 members (10-BM) in responses to the phase shifts of the two projected IPO indices.

Finally, using the IPO-constrained precipitation, the future risk of megadrought events over eastern China at the decadal scale can be projected (Fig. 4). To exclude the influence of increased precipitation due to global warming, the linear trend of projected precipitation is removed ("Detrended in Fig. 4"), and the threshold for identifying a megadrought event (mentioned in Methods) is set to -0.5σ for 2021–2080. To facilitate comparisons with historical period, another group of future risk are calculated based on projected precipitation changes with linear trend ("With trend" in Fig. 4), and the threshold for identifying a megadrought event is set to -0.5σ for 1951–2010. It's worth noting that the comparisons of future risk are based on the constrained and pre-constrained precipitation from 10-BM and 50-member, respectively (Fig. 4). Because the frequency being calculated in a 20-year window, the missing values exist in the first and last 10 years in the future period (2021–2080).

In the detrend precipitation time series, the projected risk of megadrought events over NC shows a great difference between pre-constrained and constrained precipitation for the 2040s to 2060s (Fig. 4a). The lowest risk occurs in early 2040s with the minimums of 0.0056, 0.0078 in BM-IPO and WA-IPO, respectively. The highest risk occurs in 2050s to 2060s with the maximums of 0.0280 and 0.0256 in BM-IPO and WA-IPO, respectively. However, the change of pre-constrained risk remains relatively horizontal during the future period with an average of 0.0175, showing low skill on future megadrought projection using simple ensemble mean. In the time series of precipitation with linear trends kept, due to the monotonous increasing trend of projected NC precipitation, the megadrought risk shows a trend with gradual decline from 2021 to 2080, particularly in pre-constrained results (Fig. 4c). However, after the constraining, the risks have some fluctuations and resemble to the detrend results. For example, the lower risk still occurs in 2040s with the valleys of 0.0069, 0.0079 in BM-IPO and WA-IPO, respectively. The

higher risk still occurs in 2050s to 2060s with the peaks of 0.0174 and 0.0201 in BM-IPO and WA-IPO, respectively.

The change of megadrought risk over YRV shows a reserved phase of risk of NC according to the opposite relationship with IPO. Thus, in the detrend precipitation time series, the highest risk occurs in 2030s to 2040s with maximums of 0.0223 and 0.0209 in BM-IPO and WA-IPO, respectively. The lowest risk occurs in 2050s with minimums of 0.0088 and 0.0096 in BM-IPO and WA-IPO, respectively. The change of pre-constrained risk also remains relatively horizontal during the future period with average of 0.0169. In the time series of precipitation with linear trend kept, the megadrought risk also shows a trend with gradual declined trend, but low and high risks still appear in 2040s and 2050s, respectively.

To sum up, the constraint shows that NC will have a low drought risk in the 2040s, which is dominated by the projected positive IPO phase. On the contrary, with the projected negative phase of IPO, 2050s and 2060s, the NC precipitation will decrease, leading to an increase in drought risks. In YRV, there are higher megadrought risks in 2030s and 2040s, and lower risks in the 2050s. In spite of the increasing trends in projected precipitation over NC and YRV, when only taking the IPO-constrained precipitation variability into consideration, the megadrought risk will arise.

Conclusions And Discussions

In this study, large ensemble from the CESM2-LE were used to project the risk of decadal megadrought over eastern China in future period (2021–2080). First, the comparison between 15 CMIP6 models and 50 CESM2-LE members suggested that, under the same scenario, internal variability contributes a large part of the uncertainty in simulated decadal precipitation variability over NC and YRV. IPO is the major factor of internal variability dominating the decadal precipitation variability over eastern China during both historical period (1951–2010) and future period (2021–2080). Then, the fraction of IPO-related uncertainty is calculated based on linear regression between IPO and decadal precipitation over eastern China. It's shown that the IPO-related uncertainty accounted for about 38.7% (35.7%) of the total internal uncertainty over NC (YRV) during historical period, and about 31.1% (29.1%) of the total internal uncertainty over NC (YRV) during future period (2021–2080). A constraint-based on IPO is applied to generate a more reliable decadal-scale precipitation. Finally, the future risk of decadal megadrought over eastern China is projected based on the IPO-constrained precipitation. It's found that NC will have a high megadrought risk in the 2050s to 2060s, and YRV will have a high megadrought risk in 2030s to 2040s. These findings about reliable megadrought risk projection will help government to develop sustainable strategies for future decades.

Methods

Observational data and model simulations. In this study, observed gridded monthly precipitation data is from the Global Precipitation Climatology Center (GPCC) version 2018 with a horizontal resolution of 0.5 $^\circ \times 0.5^\circ$ [49]. Observed monthly SST data is from the National Oceanic and Atmospheric Administration

(NOAA) Extended Reconstructed Sea Surface Temperatures (ERSST) Version 5 with a horizontal resolution of $2.0° \times 2.0°$ [50]. Both observed data cover the study period (1951−2010).

To estimate the total uncertainties in model simulation, the historical (1850−2014) and SSP3-7.0 (2015−2100) all-forcing simulation of 15 models from the Coupled Model Intercomparison Project Phase 6 (CMIP6; ref. [51]) (Table S1 in Supporting Information) are analyzed. The total uncertainties include both uncertainty due to internal variability and uncertainty due to model structure differences in each scenario[19].

To isolate the role of internal variability in uncertainty, the large ensemble (50 members) of historical (1850−2014) and SSP3-7.0 (2015−2100) all-forcing simulation from the Community Earth System Model Version 2 Large Ensemble (CESM2-LE; ref. [46]) with $1.0° \times 1.0°$ horizontal resolution are used in this study. Large size of simulations from different members based on the same model aims to ensure that different members are driven by the same external forcing but differ in their initial conditions. Thus, the spread among different members can represent the uncertainty due to internal variability[45]. The ensemble mean of all the members is the climate change responses to external forcing. All the model outputs are interpolated to a 73×144 global grid before the calculation.

Definitions of uncertainties. Since the internal uncertainty represents the uncertainty induced by the internal variability, which independent to external forcing, the internal uncertainty can be defined as the standard deviations (σ) of CESM2-LE ensemble under the same scenario. The inter-model uncertainty represents different responses among the models in the climate changes to the same radiative forcing. The scenario uncertainty represents the different scenarios in future emissions of GHGs, which is not considered in this study. Thus, the total uncertainty is defined as standard deviations of CMIP6 ensemble. These definitions are consistent with previous works that also used large ensemble to constrain the projected uncertainty[44,45].

Decadal megadrought definition. Megadrought is usually described as decadal hydroclimate variability, and is more severe and prolonged than observed droughts in previous studies[7,17,52]. Here, by referring to ref. [7], we use $−0.5\sigma$ of precipitation change over period of 1951−2010 (the historical period) as an exceedance threshold on the 11-year lowpass filtered standardized precipitation time series in each member. Moreover, to exclude the influence of increased precipitation due to global warming, the period is changed to 2021−2080 (the future period) with detrended precipitation.

Thus, a megadrought event is identified as period with precipitation lower than the threshold. The megadrought risk is defined as the fraction of years included in megadrought conditions and total year of the whole in a study period[7]. The magnitude of a megadrought event is defined as the mean of standardized precipitation anomalies during the megadrought event.

Emergent constraint based on IPO. First, the IPO index is defined as the differences of the region-averaged SST anomalies in the tropical central-eastern Pacific (10°S to 10°N, 170°E to 90°W) and the mean of the

northwestern (25°N to 45°N, 140°E to 145°W) and southwestern (40°S to 15°S, 150°E to 160°W) Pacific Ocean, following previous studies[53,54].

Then, standardized precipitation is linearly regressed to IPO index to obtain IPO related component of precipitation.

$$pr_{original}\left(i\right) = r_{pr,IPO}\left(i\right) \times IPO\left(i\right) + pr_{IPO-unrelated}\left(i\right), i = 1,2,\ldots,49,50$$

1

The residual part of linear regression is precipitation change without IPO influence (IPO-unrelated component). The regressed part is precipitation change with IPO influence (IPO-related component).

Next, to eliminate the uncertainty of IPO simulation on precipitation change over eastern China, a fixed IPO influence is added to the residual part. The fixed IPO influence is discussed in section 3.3.

$$r_{pr,IPO}\left(i\right) \times IPO\left(fixed\right) + pr_{IPO-unrelated}\left(i\right) = pr_{constrained}\left(i\right), i = 1,2,\ldots,49,50$$

2

The coefficient of determination (R^2) is used to estimate the proportion of total variation in precipitation that can be explained by the IPO based on above regressed relationship (Eq. 1).

$$R^2\left(i\right) = \frac{TSS\left(i\right) - RSS\left(i\right)}{TSS\left(i\right)} = \frac{ESS\left(i\right)}{TSS\left(i\right)}, i = 1,2,\ldots,49,50$$

3

Total sum of square (TSS) can be regarded as the variance of original precipitation for each member, residual sum of square (RSS) is variance of IPO-unrelated precipitation, and explained sum of square (ESS) is variance of IPO-related precipitation.

Declarations

Data Availability Statement

Author contributions

Y.Q. and L.N. designed the research. Y.Q. performed the analysis, drew all the figures, and wrote the first draft of the paper. L.N. modified the draft. L.L. and Z.L. provided comments on the analysis. All authors discussed and commented on the paper.

Competing Interests

the Authors declare no Competing Financial or Non-Financial Interests.

References

1. Fu, C. & Ma, Z. Global Change and Regional Aridification. *Chinses Journal of Atmospheric Sciences (in Chinses)*, 32, 752-760 (2008).

2. Yuan, X., Ma, Z., Pan, M. & Shi, C. Microwave remote sensing of short-term droughts during crop growing seasons. *Geophys. Res. Lett.* 42, 4394–4401. https://doi.org/10.1002/2015GL064125 (2015).

3. IPCC. Climate change 2021: the physical science basis [M/OL]. 2021 [2021-08-06]. https://www.ipcc.ch/report/ar6/wg1/#FullReport.

4. Cook, B. I., Mankin, J. S., Marvel, K., Williams, A. P., Smerdon, J. E. & Anchukaitis, K. J. Twenty-first century drought projections in the CMIP6 forcing scenarios. *Earth's Future*. **8**, e2019EF001461. https://doi.org/10.1029/2019EF001461 (2020).

5. Dai, A. Increasing drought under global warming in observations and models. *Nature Climate Change*. **3**. 52-58. https://doi.org/10.1038/nclimate1633 (2013).

6. Ning, L., Riddle, E. & Bradley, R. S. Projected changes in climate extremes over the northeastern United States. *Journal of Climate*, 28, 3289–3310. https://doi.org/10.1175/jcli-d-14- 00150.1 (2015).

7. Stevenson, S., Coats, S., Touma, D., Cole, J., Lehner F., Fasullo, J. & Otto-Bilesner, B. Twenty-first century hydroclimate: A continually changing baseline, with more frequent extremes. *Proceedings of*

the National Academy of Sciences, **199**, e2108124119. https://doi.org/10.1073/pnas.2108124119 (2022).

8. Li, C., Zwiers, F., Zhang, X., Li, G., Sun, Y. & Wehner, M. Changes in Annual Extremes of Daily Temperature and Precipitation in CMIP6 Models. *J. Clim.,* 34, 3441-3460. https://doi.org/10.1175/JCLI-D-19-1013.1 (2021).

9. Wang, L., Wang, W., Du, H., Shen, X., Wu, Z., Ma, S., Liu, Z. & Jiang, M. Was Warming Amplified Under Drought Conditions Across China in Observations and Future Projections? *Earth's Future*, **10**, e2021EF002614. https://doi. org/10.1029/2021EF002614 (2022).

10. Chen, L., Wang, G., Miao, L., Gnyawali, K. R., Li. S., Amankwah, S. O. Y., Huang, J., Lu, J. & Zhan, M. Future drought in CMIP6 projections and the socioeconomic impacts in China. *International Journal of Climatology*, 41, 4151-4170. https://doi.org/ 10.1002/joc.7064 (2021).

11. Li, W., Pan, R., Jiang, Z., Chen, Y., Li, L., Luo, J., Zhai, P., Shen, Y. & Yu, J. Future Changes in the Frequency of Extreme Droughts over China Based on Two Large Ensemble Simulations. *J. Clim.,* 34, 6023-6035. https://doi.org/ 10.1175/JCLI-D-20-0656.1 (2021).

12. Xu, Y., Zhang, X., Hao, Z., Hao, F. & Li, C. Projections of future meteorological droughts in China under CMIP6 from a three-dimensional perspective. Agricultural Water Management 252, 106849. https://doi.org/10.1016/j.agwat.2021.106849 (2021).

13. Fu, C. & An, Z. Study of aridification in northern China——A global change issue facing directly the demand of nation. *Earth Science Frontiers*, 9, 271–275 (2002).

14. Zhang, L., Zhou, T., Wu, P. & Chen, X. Potential predictability of North China summer drought. *Journal of Climate*, 32, 7247–7264. https://doi.org/10.1175/jcli-d-18-0682.1 (2019).

15. Wang, B., Jin, C. & Liu, J. Understanding Future Change of Global Monsoons Projected by CMIP6 Models. *J. Clim.*, **33**, 6471-6489, https://doi.org/10.1175/JCLI-D-19-0993.1 (2020).

16. Knutti, R. & Sedlacek, J. Robustness and uncertainties in the new CMIP5 climate model projections. *Nature Climate Change*, **3**, 369–373. https://doi.org/10.1038/nclimate1716 (2013).

17. Ault, T. R., Mankin, J. S., Cook, B. J. & Smerdon, J. E. Relative impacts of mitigation, temperature, and precipitation on 21st-century megadrought risk in the American Southwest. *Sci. Adv*. **2**, e1600873 (2016).

18. Ukkola, A. M., De Kauwe, M. G., Roderick, M. L., Abramowitz, G. & Pitman, A. J. Robust future changes in meteorological drought in CMIP6 projections despite uncertainty in precipitation. *Geophysical Research Letters*, **46**, e2020GL087820. https://doi.org/10.1029/2020GL087820 (2020).

19. Hawkins, E. & Sutton, R. The Potential to narrow uncertainty in regional climate predictions. *Bull. Am. Meteorol. Soc*. 90, 1095–1108 (2009).

20. Lehner, F., Deser, C., Maher, N., Marotzke, J., Fischer, E. M., Brunner, L., Knutti, R. & Hawkins, E. Partitioning climate projection uncertainty with multiple large ensembles and CMIP5/6. *Earth Syst. Dynam*. **11**, 491–508. https://doi.org/10.5194/esd-11-491-2020 (2020).

21. Chai, Y., Yue, Y., Slater, L. J., Yin, J., Borthwick, A. G., Chen, T. & Wang, G. Constrained CMIP6 projections indicate less warming and a slower increase in water availability across Asia. *Nature*

Communications. **13**, 4124, https://doi.org/10.1038/s41467-022-31782-7 (2022).

22. Chen, Z., Zhou, T., Chen, X., Zhang, W., Zhang, L., Wu, M. & Zou, L. Observationally constrained projection of Afro-Asian monsoon precipitation. *Nature Communications.* **13**, 2552, https://doi.org/10.1038/s41467-022-30106-z (2022).

23. Huang, D., Zhu, J., Zhang, Y. & Huang, A. Uncertainties on the simulated summer precipitation over Eastern China from the CMIP5 models. *J. Geophys. Res. – Atmos.* **118**, 9035–9047, https://doi.org/10.1002/jgrd.50695 (2013).

24. Coast, S., Smerdon, J. E., Cook, B. I. & Seager, R. Are Simulated Megadroughts in the North American Southwest Forced? *J. Clim.,* 28, 124-142. https://doi.org/ 10.1175/JCLI-D-14-00071.1 (2015).

25. Qin, Y., Ning, L., Chen, K., Liu, J. & Yan, M. Assessment of PMIP3 model simulations of megadroughts over the eastern China during the last millennium. *International Journal of Climatology*, **40**, 5188–5207. https://doi.org/10.1002/joc.6513 (2020).

26. Ning, L., Liu, J., Wang, B., Chen, K., Yan, M., Jin, C. & Wang, Q. Variability and mechanisms of megadroughts over east- ern China during the last millennium: a model study. *Atmosphere*, 10, 1–26. https://doi.org/10.3390/atmos10010007 (2019).

27. Stevenson, S., Overpeck, J. T., Fasullo, J., Coast, S., Parsons, L., Bliesner-Otto, B., Ault, T., Loope, G. & Cole, J. Climate Variability, Volcanic Forcing, and Last Millennium Hydroclimate Extremes. *J. Clim.,* 31, 4309-4327. https://doi.org/ 10.1175/JCLI-D-17-0407.1 (2018).

28. Chen, K., Ning, L., Liu, Z., Liu, J., Yan, M., Sun, W., Yuan, L., Lv, G., Li, L., Jin, C., & Shi, Z. One drought and one volcanic eruption influenced the history of China: The late Ming Dynasty mega-drought. *Geophysical Research Letters*, 47, e2020GL088124. https://doi.org/10.1029/2020GL088124U (2020).

29. Qin, Y., Ning, L., Li, L., Liu, Z., Liu, J., Yan, M., Chen, K., Xue, J., Wang, L. & Li, C. Assessing the recent multi-decadal scale aridification over the Northern China from a historical perspective. *J. Geophys. Res. – Atmos.* **127**, e2021JD035622. https://doi. org/10.1029/2021JD035622 (2022).

30. Xue, J., Ning, L., Liu, Z., Qin, Y., Chen, K., Yan. M., Liu, J., Wang, L., & Li, C. The combined influences of Solar Radiation and PDO on Precipitation over Eastern China during the last millennium. *Clim. Dyn.* https://doi.org/10.1007/s00382-022-06372-4 (2022).

31. Wang, L., Ning, L., Chen, K., Yan, M., Liu, J., Liu, Z., Qin, Y., Xue, J. & Li, C. Influence and mechanism of solar radiation intensity on the interdecadal variability of strong Meiyu events during historical periods. *Science China Earth Sciences*, 65, https://doi.org/10.1007/s11430-021-9952-0 (2022).

32. Power, S., Casey, T., Folland, C., Colman, A. & Mehta, V. Interdecadal modulation of the impact of ENSO on Australia. *Climate Dynamics*, **15**, 319–324. https://doi.org/10.1007/s003820050284 (1999).

33. Mantua, N. J., Hare, S. R., Zhang, Y., Wallace, J. M., & Francis, R. C. (1997), A Pacific interdecadal climate oscillation with impacts on salmon production. *Bulletin of the American Meteorological Society*, **78**, 1069–1079. https://doi.org/10.1175/1520-0477(1997)078<1069:APICOW>2.0.CO;2

34. Dong, B. & Dai, A.The influence of the Interdecadal Pacific Oscillation on Temperature and Precipitation over the Globe. *Clim, Dyn*, **45**, 2667-2681. https://doi.org/ 10.1007/s00382-015-2500-x (2015).

35. Hartmann, B. & Wendler, G. The significance of the 1976 Pacific climate shift in the climatology of Alaska. *J. Clim*. **18**,4824−4839 (2005).

36. Meehl, G. A. & Hu, A. Megadroughts in the Indian monsoon region and southwest North America and a mechanism for associated multidecadal Pacific sea surface temperature anomalies. *J. Clim*. **19**, 1605−1623 (2006).

37. Ning, L. & Bradley, R. S. Winter precipitation variability and corresponding teleconnections over northeastern United States. *Journal of Geophysical Research − Atmospheres*, 119(13), 7931−7945. https://doi.org/10.1002/2014JD021591 (2014).

38. Si, D. & Hu, A. Internally Generated and Externally Forced Multidecadal Oceanic Modes and Their Influence on the Summer Rainfall over East Asia. *J. Clim*. **30**, 8299−8316. https://doi.org/10.1175/JCLI-D-17-0065.1 (2017).

39. Yang, Q., Ma, Z., Fan, X., Yang, Z., Xu, Z. & Wu, P. Decadal modulation of precipitation patterns over east China by sea surface temperature anomalies. *Journal of Climate*, 30, 7017−7033. https://doi.org/10.1175/jcli-d-16-0793.1 (2017).

40. Xue, J., Ning, L., Qin, Y., Chen, K. M. & Liu, J. Comparisons on characteristics and mechanisms of the decadal megadroughts over eastern China between MCA and LIA. *International Journal of Climatology*, **41**, 1985−1997. https://doi.org/10.1002/joc.6942 (2020).

41. Zhang, Z., Sun, X. & Yang, X. Understanding the interdecadal variability of East Asian Summer Monsoon precipitation joint influence of three oceanic signals. *Journal of Climate*, 31, 5485−5506. https://doi.org/10.1175/JCLI-D-17-0657.1 (2018).

42. Ma, Z. The interdecadal trend and shift of dry/wet over the central part of North China and their relationship to the Pacific decadal oscillation (PDO). *Chinese Science Bulletin*, **52**, 2130−2139. https://doi.org/10.1007/s11434-007-0284-z (2007).

43. Yang, X., Xie, Q., Zhu, Y., Sun, X. & Guo, Y. Decadal-to-interdecadal variability of precipitation in North China and associated atmospheric and oceanic anomaly patterns. *Chinese Journal of Geophysics*, **48**, 789−797. https://doi.org/10.1111/j.1745-7254.2005.00209.x (2005).

44. Huang, X., Zhou, T., Dai, A., Li, H., Li, C., Chen, X., Lu, J., Von storch, J. & Wu, B. South Asian summer monsoon projections constrained by the interdecadal Pacific oscillation. *Sci. Adv*. 6, eaay6546. https://doi.org/10.1126/sciadv.aay6546 (2020).

45. Dong, L., Leung, L. R., Song, F. & Lu, J. Uncertainty in El Niño-like warming and California precipitation changes linked by the Interdecadal Pacific Oscillation. *Nature Communications*. 12, 6484, https://doi.org/10.1038/s41467-021-26797-5 (2021).

46. Rodgers, K. B., Lee, S., Rosenbloom N., Timmermann, A., Danabasoglu G., Deser, C., Edwards, J., Kim, J., Simpson, I. R., Stein, K., Stuecker, M. F., Yamaguchi, R., Bódai, T., Chung, E., Huang, L., Kim, W. M., Lamarque, J., Lombardozzi, D. L., Wieder, W. R. & Yeager, S. G. Ubiquity of human-induced changes in

climate variability. *Earth Syst. Dynam.*, **12**, 1393–1411. https://doi.org/10.5194/esd-12-1393-2021 (2021).

47. Yang, Q., Ma, Z. & Xu, B. Modulation of monthly precipitation patterns over East China by the Pacific Decadal Oscillation. *Climate Change*. **144**. 405-417. https://doi.org/10.1007/s10584-016-1662-9 (2017).

48. Ma, Z. Dry/wet variation and its relationship with regional warming arid-regions of northern China. *Chinese Journal of Geophysics*, 48(5), 1011–1018. https://doi.org/10.1002/cjg2.752 (2005).

49. Schneider, U., Becker, A., Finger, P., Meyer-Christoffer, A., Ziese, M. & Rudolf, B. GPCC's new land surface precipitation climatology based on quality-controlled in situ data and its role in quantifying the global water cycle. *Theoretical and Applied Climatology*, 115, 15–40. https://doi.org/10.1007/s00704-013-0860-x (2014).

50. Huang, B., Thorne, P. W., Banzon, V. F., Boyer, T., Chepurin, & G., Lawrimore, J. H., et al. Extended reconstructed sea surface temperature, version 5 (ERSSTv5). *Upgrades, Validations, and Intercomparisons*, 30, 8179–8205. https://doi.org/10.1175/JCLI-D-16-0836.1 (2017).

51. Eyring, V., Bony, S., Meehl, G. A., Senior, C. A., Stevens, B., Stouffer, R. J. & Taylor, K. E. Overview of the Coupled Model Intercomparison Project Phase 6 (CMIP6) experi- mental design and organization. *Geosci. Model Dev.*, 9, 1937– 1958, https://doi.org/10.5194/gmd-9-1937-2016 (2016).

52. Cook, B. I., Cook, E. R., Smerdon, J. E., Seager, R., Williams, A. P., Coats, S., Stahle, D. W. & Diaz, J. V. North American megadroughts in the common era: reconstructions and simula- tions. *Wiley Interdisciplinary Reviews: Climate Change*, 7, 411–432. https://doi.org/10.1002/wcc.394 (2016).

53. Henley, B. J., Gergis, J., Karoly, D. J., Power, S., Kennedy, J. & Folland, C. K. A tripole index for the Interdecadal Pacific Oscillation. *Climate Dynamics*, 45(11–12), 3077–3090. https://doi.org/10.1007/s00382-015-2525-1 (2015).

54. Hua, W., Dai, A. & Chen, H. Little influence of Asian anthropogenic aerosols on summer temperature in Central East Asia since 1960. *Geophysical Research Letters*, **49**, e2022GL097946. https://doi.org/10.1029/2022GL097946 (2022).
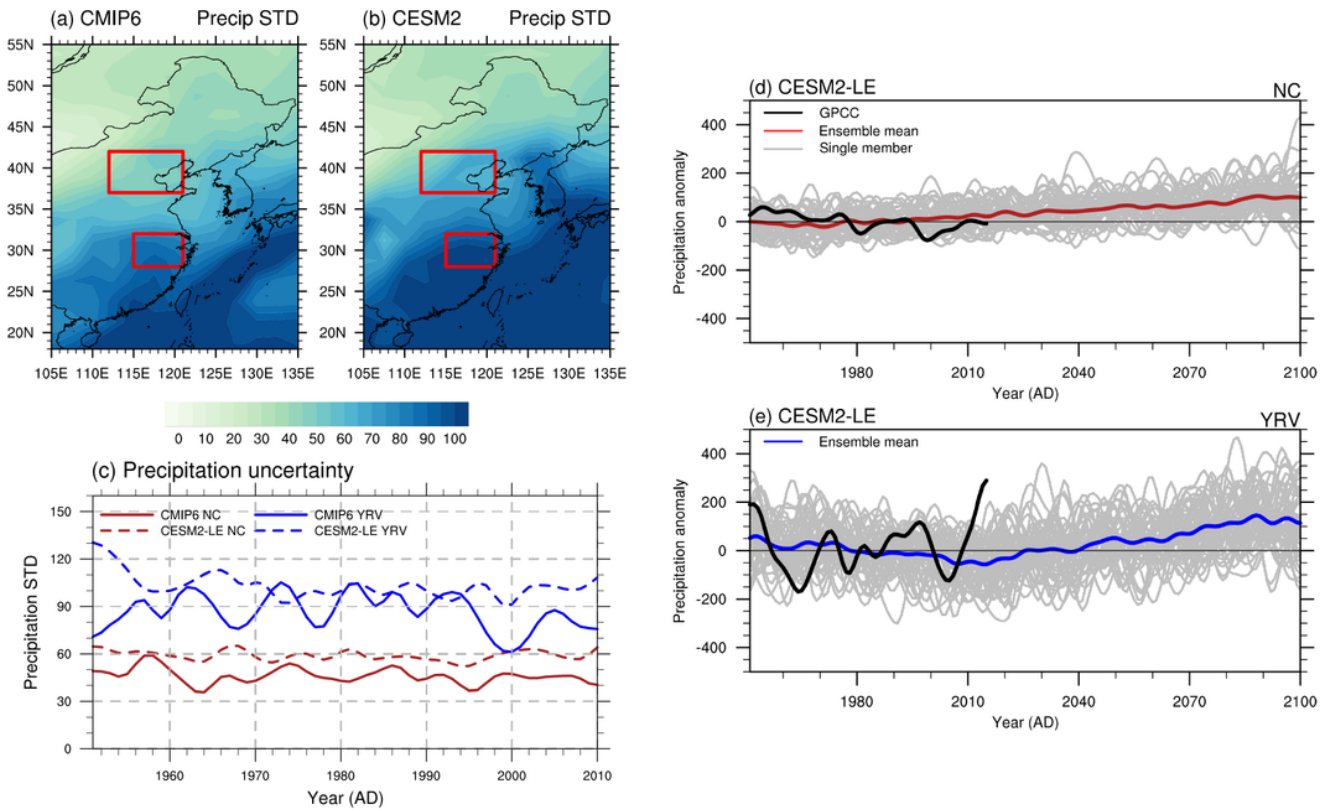
Figures

Figure 1

Uncertainties in simulated decadal scale precipitation over NC and YRV. (a) Total uncertainty of decadal scale precipitation changes during 1951-2010 based on 15 models of CMIP6 (unit: mm/year). **(b)** Internal uncertainty based on 50 members of CESM2-LE. **(c)** Time series of total uncertainty (solid line) and internal uncertainty (dash line) over NC (red line) and YRV (blue line) based on CMIP6 and CESM2-LE ensembles (unit: mm/year). **(d)** and **(e)** Time series of annual mean of 11-year lowpass filtered precipitation anomalies relative to 1951-2010 over NC and YRV from GPCC during the period 1951-2016 (thick black lines) and from 50 members of CESM2-LE simulations during the period 1951-2100 (unit: mm/year).
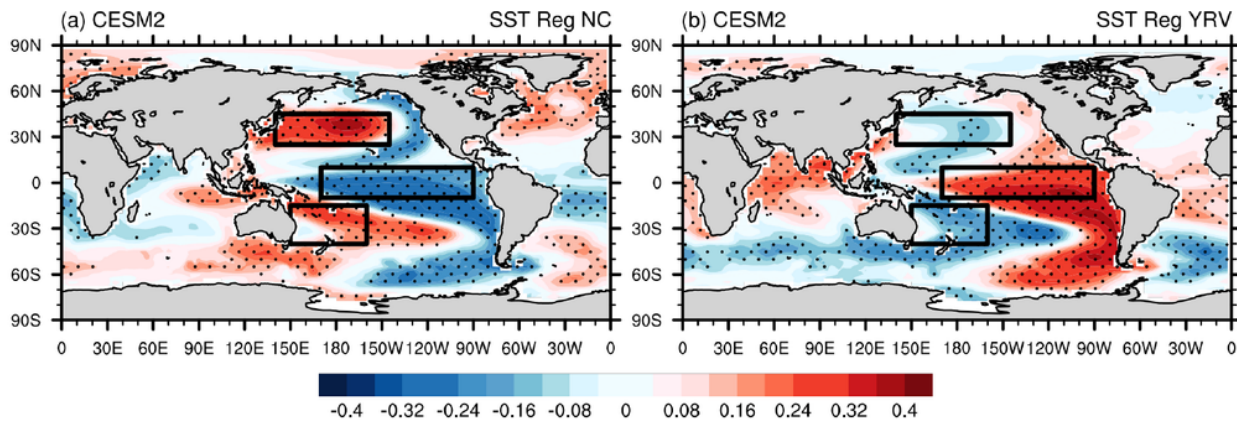

Figure 2

Relationship between the precipitation over eastern China and IPO. Ensemble mean regressions of SST onto NC (**a**) and YRV (**b**) precipitation during 1951-2010 from the 50 CESM2-LE members. Stippling indicate that differences are significant at 95% level based on Student t-test.
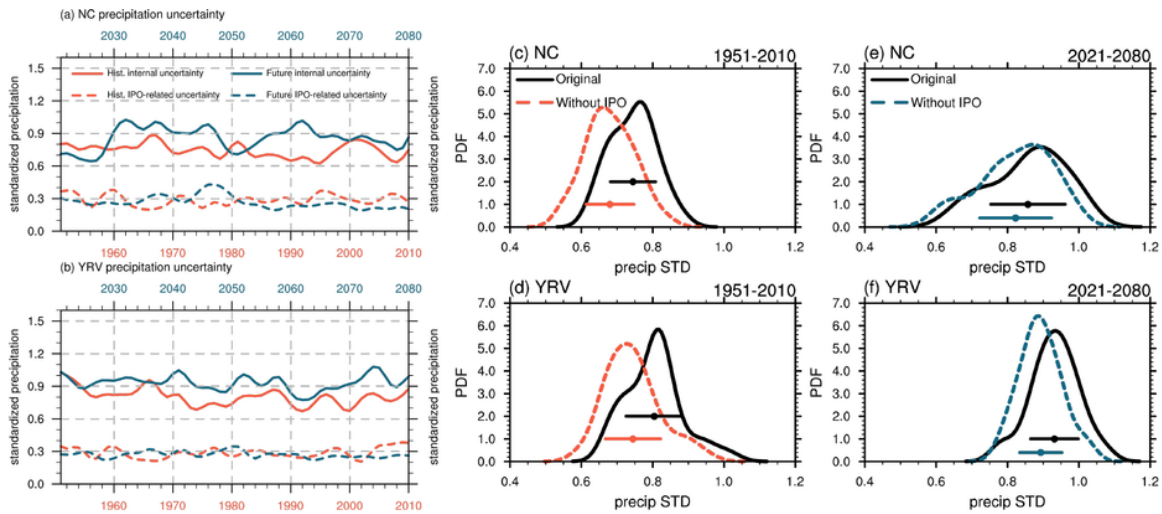

Figure 3

IPO-related contribution to internal uncertainty. Time series (**a-b**) of internal uncertainty (solid line) and IPO-related uncertainty (dash lines) in NC (**a**) and YRV (**b**) precipitation during historical period (1951-2010, red lines) and future period (2021-2080, blue line). Probability distributions (**c-f**) of standard deviation (STD) of pre-constrained (black lines) and without IPO-influenced (colored lines) precipitation over NC (**c, e**) and YRV (**d, f**). The dots and bars denote the ensemble means and ±s of the distribution.
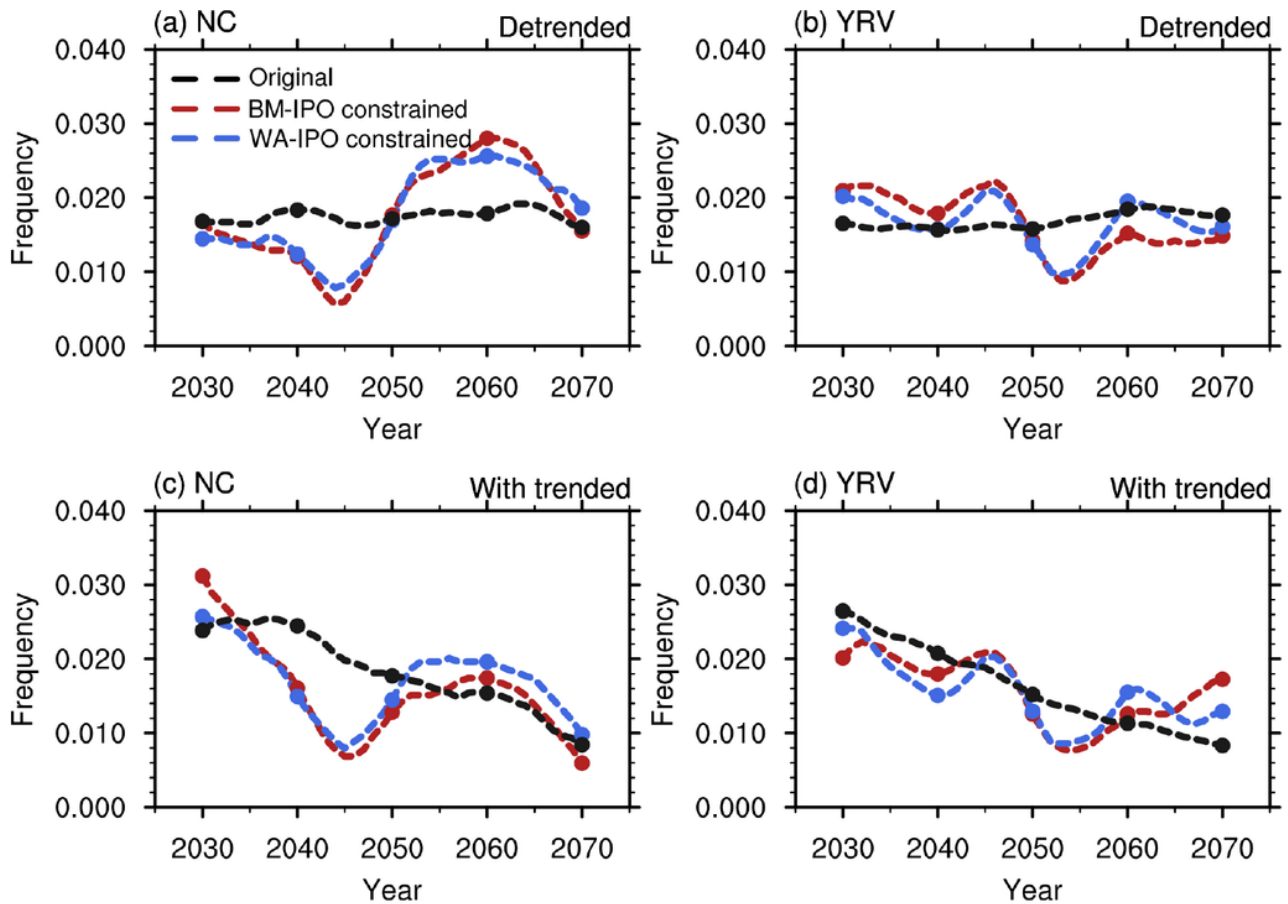
Figure 4

Future risk of megadrought events based on original (pre-constrained) and constrained precipitation.
Frequencies distribution of megadrought events calculated in 20-year window for period 2020-2070 over
NC (**a, c**) and YRV (**b, d**) from detrended precipitation change (**a, b**) and precipitation change with trend (**c,
d**). Black line denotes frequencies of megadrought events based on original (pre-constrained)
precipitation; Red line denotes frequencies of megadrought events based on BM-IPO constrained
precipitation; Blue line denotes frequencies of megadrought events based on WA-IPO constrained
precipitation.

Supplementary Files

This is a list of supplementary files associated with this preprint. Click to download.

- YanminSupplementarymaterial.pdf